A time-domain simulation of an oscillating water column with irregular waves

Weoncheol Koo*[1] and Moo-Hyun Kim[2]

[1]School of Naval Architecture and Ocean Eng., Univ. of Ulsan, 680-749, Ulsan, Korea
[2]Department of Civil Engineering, Texas A&M Univ., College Station, TX,77843, USA

Abstract. A time-domain simulation of a land-based Oscillating Water Column (OWC) with various irregular waves as a form of PM spectrum is performed by using a two-dimensional fully nonlinear numerical wave tank (NWT) based on the potential theory, mixed Eulerian-Lagrangian (MEL) approach, and boundary element method. The nonlinear free-surface condition inside the OWC chamber was specially devised to describe both the pneumatic effect of the time-varying pressure and the viscous energy loss due to water column motions. The quadratic models for pneumatic pressure and viscous loss are applied to the air and free surface inside the chamber, and their numerical results are compared with those with equivalent linear ones. Various wave spectra are applied to the OWC system to predict the efficiency of wave-energy take-off for various wave conditions. The cases of regular and irregular waves are also compared.

Keywords: oscillating water column; numerical wave tank; irregular waves; pneumatic chamber, equivalent linear damping; viscous energy loss; available power

1. Introduction

During the past decades, many wave-energy converters have been proposed, developed, and tested. One of the most promising concepts is the oscillating water column (OWC) device with pneumatic power take-off by air turbines. The incident wave causes the water column inside chamber to move up and down and compress and expand the air at its top. The bi-directional airflows generated through the narrow outlets drive turbines to generate electricity (e.g., Masuda *et al*. 1979, Heath *et al*. 2000, Josset and Clement 2007).

In this study, by using a two-dimensional fully nonlinear boundary element (BE) numerical wave tank (NWT) in the time domain (Koo and Kim 2004, Kim and Koo 2005), we investigated the hydrodynamic performance of a land-based OWC plant with irregular wave inputs. The developed NWT technique was based on potential theory with fully nonlinear free-surface conditions and a mixed Eulerian-Lagrangian (MEL) time-marching approach, which has been verified against various experimental results, including nonlinear waves and fixed or floating bodies (Koo and Kim 2004). The NWT was further extended to include interactions between oscillatory air and surface elevation inside the chamber, and the energy loss due to viscosity from the oscillation of the water column in

---

*Corresponding author, Professor, E-mail: wckoo@ulsan.ac.kr

regular incident waves (Koo and Kim 2010). Koo and Kim (2011) showed preliminary results of the numerical simulation of OWC in irregular waves. The model of pneumatic chamber and water column movement is based on the assumption of linear or quadratic relations between chamber pressure and air-duct velocity, which was experimentally supported by Gato and Falcao (1988) and Suzuki and Arakawa (2000).

The dimension of the present OWC model is the same as that used in the experiment of Liu *et al.* (2008). The numerical results from the developed NWT with regular wave inputs were compared with their experiments in the previous study of Koo and Kim (2010), including water column movement, viscous damping effects, hydrodynamic efficiency, and free-surface pattern. The comparisons were reasonably good with tuned viscous and pneumatic coefficients.

After verification for the regular wave input, the developed numerical tool is used for irregular wave input represented by two-parameter PM (Pierson-Moskowits) spectra with various significant wave heights and periods. A special frontal-damping zone is implemented in front of the wave maker so that it can dampen the differences between the incident waves and the total irregular waves including reflected waves from OWC. As far as authors know, the fully nonlinear simulations for OWCs for irregular waves with nonlinear pneumatic and viscous parameters have never been published in the open literature. In addition, the fully nonlinear NWT-OWC simulations are also applied for both regular and irregular waves with equivalent linear coefficients to check the validity of such a simplified procedure. Compared to incident wave amplitudes, the free-surface fluctuation inside the chamber is found to be significantly higher especially near the resonance frequencies. In order to compare the hydrodynamic performance of OWC in irregular waves with the regular-wave case, the chamber-elevation RAO (response amplitude operator) is obtained from the square root of the spectral ratio of chamber-elevation spectrum to incident-wave spectrum.

2. Mathematical formulation

In order to simulate nonlinear free-surface elevations of a land-based OWC with irregular wave input, the Laplace equation is used as a governing equation with velocity potential and the corresponding boundary conditions to solve a boundary integral equation. The details of the fully-nonlinear NWT simulation technique are given in Koo and Kim (2004). The present fully nonlinear free-surface condition cannot be used when any portion of free surface has double values by overturning and splashing. The mathematical formulation and numerical implementation of the chamber free-surface model with pneumatic effect and viscous energy loss are explained in Koo and Kim (2010) and Koo *et al.* (2006). In Koo and Kim (2010), the numerical simulations were also verified against the experimental results of Liu *et al.* (2008). In this paper, only the key features of them are presented.

A frontal damping zone in front of the wave maker is necessary to prevent the re-reflection of the reflected waves from the wave maker for a long time-domain simulation. This damping scheme must be designed to dampen only the reflected waves from the OWC, while preserving the original incident waves. Therefore, the damping was applied only to the difference between the total waves and the incident waves, and the corresponding boundary condition can be expressed as

$$\frac{\delta\phi}{\delta t} = -g\eta - \frac{1}{2}|\nabla\phi|^2 + \nabla\phi \cdot \vec{v} + \mu_1\left(\frac{\partial\phi}{\partial n} - \frac{\partial\phi}{\partial n}*\right) \tag{1}$$

$$\frac{\partial \eta}{\partial t} = \frac{\partial \phi}{\partial z} + \mu_2(\eta - \eta^*) \tag{2}$$

where μ_1 and μ_2 denote artificial damping coefficients, and the values of $(\partial \phi / \partial n)^*$ and η^* are to be computed with the same computational condition in the absence of bodies. However, in the case of moderate nonlinear incident waves, proper analytic solutions (e.g., linear or second-order stokes irregular waves) can be used for practical applications, as pointed out by Tanizawa and Naito (1997) and Koo and Kim (2004).

The time-varying chamber pressure influences the water column motion inside the chamber. The linear or quadratic damping terms can be used with the respective coefficients C_{dm} or D_{dm} to model the oscillatory air pressure, which also represents the energy absorption by the air turbine inside the chamber. The oscillating air pressure also causes a radiated wave from the chamber. A detailed description of the pneumatic damping system and its interactions with incident and diffracted waves is given in Koo *et al*. (2006). The linear pneumatic model is given by

$$P_{ac}(t) = \frac{C_{dm}\Delta V}{A_d \Delta t} = C_{dm}U_d(t) \tag{3a}$$

where C_{dm} is a linear damping coefficient, $\Delta V = V_t - V_{t-\Delta t}$ is the change of air volume in the chamber, A_d is the sectional area of the air duct, and $U_d(t)$ is the airflow velocity at the nozzle outlet under the assumption of incompressible air, which can be applied to relatively large air openings such as the air duct. The significance of applying damping (C_{dm}) to the air pressure is the energy absorption by the air turbine inside the chamber. This linear pneumatic model can be reasonably applied to Wells-turbine case (Gato and Falcao 1988). For other types of turbines or when the pneumatic energy is dissipated as exit kinetic energy loss at one or the other end of duct, the pressure drop may be proportional to the velocity squared. In such a case, the quadratic pneumatic term can be applied without difficulty by using the present nonlinear time-domain NWT technique. Then, the Eq. 3(a) is changed to

$$P_{ac}(t) = D_{dm}U_d(t)|U_d(t)| \tag{3b}$$

In both linear and quadratic cases, the constants of proportionality can be determined through comparison with experiments with respective exit conditions. On the other hand, energy loss in the OWC system may occur at the entrance (chamber skirt) of the chamber when incident waves surge into the chamber and move up and down like a piston. In this regard, the difference between experimental results (or VOF computation) of Liu *et al*. (2008) and the potential-fluid-based numerical results (Koo and Kim 2010) should be interpreted as energy loss due to viscosity. For instance, a typical entry head loss (or pressure drop) is expressed by

$$h_L = K_L \frac{V^2}{2g} \quad \text{or} \quad \Delta P = K_L \frac{1}{2}\rho V^2 \tag{3c}$$

where K_L is the loss coefficient and V is the flow velocity. When the loss is assumed to be

linearized so that the flow velocity is proportional to the vertical velocity of the water column ($V \approx \partial \eta / \partial t = \dot{\eta}$), then the pressure drop can be described as

$$P_v(t) = K_L^* \overline{\dot{\eta}}(t) = v \frac{\partial \phi(t)}{\partial n} \tag{3d}$$

where K_L^* and $\overline{\dot{\eta}}$ represent a modified loss coefficient and a spatial-mean surface velocity in the chamber, respectively, and v is a viscous damping coefficient. Therefore, the energy loss inside the chamber due to viscosity can be related to the viscous effects in the dynamic free-surface condition in a similar way to the energy loss from the work performed by the pneumatic pressure. The viscous loss can be represented by less pumping motion inside the chamber and it can be included in the chamber free-surface condition. Therefore, the final free-surface dynamic boundary condition inside the chamber with linear pneumatic energy extraction and linear viscous energy loss can be expressed as

$$\frac{\delta\phi}{\delta t} = -g\eta - \frac{1}{2}|\nabla\phi|^2 + \nabla\phi \cdot \vec{v} - \frac{1}{\rho}\left(C_{dm}U_d + v\frac{\partial\phi}{\partial n}\right) \tag{4}$$

Since the energy loss is related to the flow velocity and proportional to the velocity squared, when the quadratic pneumatic and viscous-loss coefficients (D_{dm} and v_q) are applied, the dynamic free surface boundary condition inside the chamber is changed to

$$\frac{\delta\phi}{\delta t} = -g\eta - \frac{1}{2}|\nabla\phi|^2 + \nabla\phi \cdot \vec{v} - \frac{1}{\rho}\left(D_{dm}U_d|U_d| + v_q\frac{\partial\phi}{\partial n}\left|\frac{\partial\phi}{\partial n}\right|\right) \tag{5}$$

2.1 Linearization of quadratic damping coefficients

The nonlinear (quadratic) pneumatic and viscous terms can only be treated by nonlinear time-domain simulation techniques. If the equivalent linearization is possible, the terms can be combined with linear frequency-domain analysis, which is in general much simpler in many aspects. In this regard, the equivalent-linearization technique for the quadratic coefficients is introduced here and its validity is examined. The equivalent linear coefficient can be derived by using the principle of equal energy dissipation per cycle by linear and quadratic damping terms. Since the energy dissipation at resonance frequency in linear and nonlinear system is same, the equivalent term can be used for moderate nonlinear waves. In the case of regular waves, the equivalent linear coefficients for pneumatic pressure and viscous damping are given by

$$C_{eqiv} = \frac{8}{3\pi}D_{dm}\omega \tag{6}$$

$$v_{eqiv} = \frac{8}{3\pi}v_q\omega \tag{7}$$

The equivalent linear coefficients for irregular wave case can be obtained by using the spectra of airflow in the nozzle outlet (Eq. (8)) and vertical free-surface velocity in the chamber (Eq. (9)), respectively.

$$C_{eqiv} = \sqrt{\frac{8}{\pi}}D_{dm}\sigma_{Ud} \tag{8}$$

$$v_{eqiv} = \sqrt{\frac{8}{\pi}} v_q \sigma_{\frac{\partial \phi}{\partial n}} \tag{9}$$

where $\sigma_{Ud} = \sqrt{\text{area of } S_{U_d}(\omega)}$ and $\sigma_{\frac{\partial \phi}{\partial n}} = \sqrt{\text{area of } S_{\frac{\partial \phi}{\partial n}}(\omega)}$, $S_{U_d}(\omega)$ and $S_{\frac{\partial \phi}{\partial n}}(\omega)$ are velocity spectra of airflow and spatial-mean vertical elevation inside the chamber.

3. Numerical results and discussions

The overview of computational domain for a land-based OWC is shown in Fig. 1. More detailed information of the OWC system is given in Table 1. To verify the present formulation and methodology, the numerical results with regular wave input were first compared with the experimental results of Liu *et al*. (2008) and the detailed comparisons were given in Koo and Kim (2010). A proper pneumatic coefficient (C_{dm} or D_{dm}) and an adequate viscous damping coefficient (v or v_q) for the chamber-duct area ratio were chosen so that the overall numerical results match well against the experimental results. Here, we applied the similar NWT computational method to assess the performance of the same kind of OWC in irregular waves. The differences in the effectiveness of the OWC in regular and irregular waves are illustrated for several different input wave spectra. The fully nonlinear free-surface simulations with nonlinear pneumatic and viscous parameters are compared with those with linear equivalent ones. To the best knowledge of authors, these kinds of fully nonlinear simulations for OWCs in irregular waves have never been published in the open literature.

Fig. 2 shows the PM spectra with various peak periods with the same significant wave height of
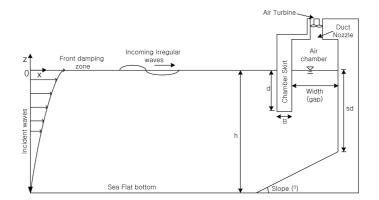

Fig. 1 Overview of the computational domain for a land-based OWC air chamber

Table 1 Calculation conditions of the numerical simulation

CASE	d(m)	B(m)	gap(m)	sd(m)	Slope(°)	h(m)	A_i(m)	Chamber-duct area ratio
Case 1	2.5	1.0	6.0	4.78	26	16	0.5	46.6

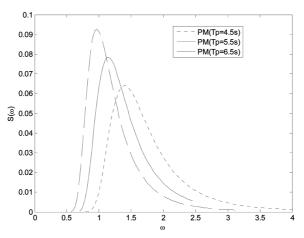Note that A_i is incident wave amplitude.

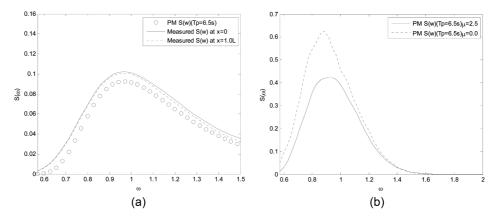Fig. 2 Comparison of PM spectrum with various peak periods (Hs = 1 m)

Fig. 3 (a) Comparison of the generated incident wave spectra at two positions inside the damping zone against the theoretical input spectrum (circle) and (b) comparison of wave spectrum measured at mid-point inside the chamber with and without frontal damping zone

1 m. As explained in the previous section, it is very important to prevent the re-reflection of the reflected irregular waves from the wave-maker position (x = 0) to accurately assess the performance of the OWT. With imposing the frontal damping zone, it is shown in Koo and Kim (2010) that the total energy within the computational domain is satisfactorily conserved for regular waves. In this regard, a specially devised frontal damping is placed in front of the wave maker to dissipate only the reflected irregular waves in the zone. The performance of the frontal damping scheme is shown in Fig. 3(a), where the incident wave spectra at two positions (x = 0 and x = 1L) within the damping zone of two wavelengths corresponding to T_p are about the same as the input theoretical spectrum. This shows that the generated incident irregular waves are little affected by the applied artificial damping, while only the reflected irregular waves are effectively dissipated within the frontal damping zone by using the present numerical scheme. The realization of the truly open boundary at the wave-maker position is very important to accurately assess the performance of Fig. 1-type OWC. For instance, the free-surface elevations inside the OWC chamber with and without the
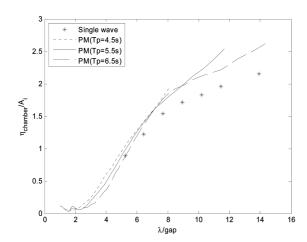
Fig. 4 Comparison of chamber-surface-elevation RAO for Case 1 with various peak periods, $D_{dm} = 0.004$, $v_q = 500$ (quadratic coefficients), Single wave (H = 1 m), PM spectrum (Hs = 1.0 m)
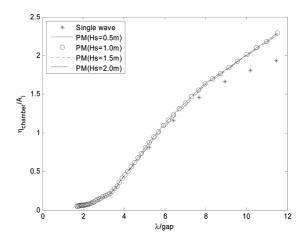

Fig. 5 Comparison of chamber-surface-elevation RAO for Case 1 with various significant wave heights, $C_{dm} = 2$, $v = 800$, Single wave (H = 1 m), PM ($T_p = 5.5$ s)

frontal damping zone are compared in Fig. 3(b).

Fig. 4 shows the comparisons of the normalized chamber-surface elevations with various peak periods of PM spectra. In this case, the quadratic pneumatic and viscous-damping coefficients of $D_{dm} = 0.004$ and $v_q = 500$ are applied. The vertical axis is the ratio of the free-surface elevation inside chamber to that of incident wave and it is obtained by the square root of the respective spectral ratio. The methodology is valid only within the range in which the incident wave spectrum is not close to zero. In other words, it is not valid outside the cut-off frequencies. In this regard, the effective range is defined for each case i.e., $0.78 \sim 4.1$ rad/s for $T_p = 4.5$ s, $0.69 \sim 3.5$ 1rad/s for $T_p = 5.5$s, and $0.57 \sim 3.14$ rad/s for $T_p = 6.5$ s. The corresponding effective wavelength bands are $3.5 \sim 83.4$ m for $T_p = 4.5$ s, $9.75 \sim 97.7$ m for $T_p = 5.5$ s, and $6.24 \sim 125.5$ m for $T_p = 6.5$ s. Since the frontal damping zone is designed within two wavelengths corresponding to Tp, it may not be very effective for component waves much longer that. In this regard, the curves for irregular waves are plotted only within narrower effective range for each Tp. The irregular wave results are also compared with the regular wave result. The chamber elevation for the regular wave is based on the wave height of 1m. It is seen that the general trend of regular- and irregular-wave results is very similar, while those of irregular waves are slightly larger. They are not necessarily identical because the applied system is quadratic and nonlinear interactions among component waves are also possible in irregular-wave cases. Nevertheless, there exist only small differences among the cases of different input spectra.

Fig. 5 shows the comparison of chamber-surface-elevation RAOs with various significant wave heights. In this case, the peak period is fixed at 5.5sec and linear viscous and pneumatic terms are applied. It is seen that the effect of wave heights on the chamber-elevation RAO is not significant for the given Hs range with the linear pneumatic and viscous coefficients. The situation may be different when the pneumatic and viscous coefficients become nonlinear (for example, quadratic model, as in Fig. 8). From these brief comparisons, it is seen that the hydrodynamic performance of the OWC in irregular waves is in general similar to that of regular waves for both linear and
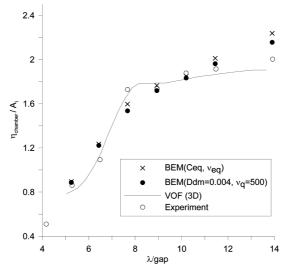
Fig. 6 Comparison of chamber surface elevation for Case 1 with quadratic coefficients ($D_{dm} = 0.004$, $v_{quad} = 500$) and linear equivalent coefficients (Table 2) in regular waves, Wave height=1 m

quadratic viscous and pneumatic models.

Fig. 6 shows the chamber surface elevation for regular waves of Case 1 as function of wave length. In this case, both quadratic pneumatic and viscous coefficients are used. With the given $D_{dm} = 0.004$ and $v_{quad} = 500$, the present NWT results correlate well against the experimental and VOF(volume of fluid) results of Liu *et al*. (2008). In the same figure, alternative simulations with the linear equivalent coefficients obtained from Eqs. (6) and (7) are also given, which is shown in Table 2. It is seen that the quadratic and equivalent linear cases agree well for the entire frequency region, which implies that the equivalent-linearization technique is a useful tool in studying the OWC performance. In particular, the equivalent linearization technique greatly simplifies the relevant statistics, and thus much more useful in case of irregular waves.

Fig. 7 shows the same case as Fig. 6 with increased incident wave height H = 1.5 m. Since the system is nonlinear with quadratic pneumatic and viscous terms, the RAOs for H = 1.5 m are different from those of H=1m. The linear equivalent coefficients are dependent on relevant response amplitudes, as shown in (6) and (7), and thus their values are different from those of Fig. 6. It is also seen that the differences between the quadratic and linear equivalent cases are increased in

Table 2 Calculated linear equivalent coefficients for regular waves

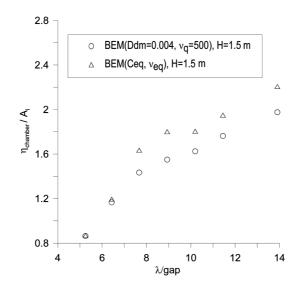| Period (sec)	C_{eq} (H = 1 m)	v_{eq} (H = 1 m)
4.5	2.20	360.3
5.0	2.49	409.6
5.5	2.51	411.2
6.0	2.42	396.0
6.5	2.27	370.2
7.0	2.07	337.4
8.0	1.72	280.1

Fig. 7 Comparison of chamber surface elevation with quadratic coefficients ($D_{dm} = 0.004$, $v_{quad} = 500$) and linear equivalent coefficients (Table 2) in regular waves of H = 1.5 m
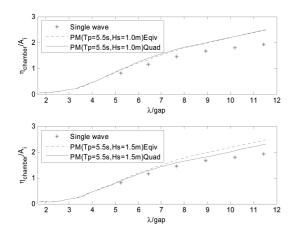

Fig. 8 Comparison of chamber surface elevation with linear equivalent coefficients ($C_{eqiv} = 1.86$, $v_{eqiv} = 304.4$) and quadratic coefficients ($D_{dm} = 0.004$, $v_{eqiv} = 500$) in irregular waves, Single wave (H = 1 m)
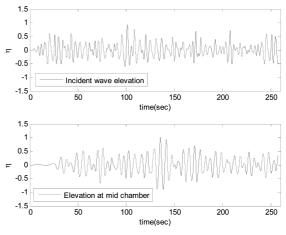
Fig. 9 Time histories of incident irregular waves (upper) and free surface at chamber midpoint (lower) with quadratic coefficients ($D_{dm} = 0.004$, $v_{quad} = 500$), PM spectrum ($T_p = 5.5$, Hs = 1 m)

higher waves due to more nonlinearities. This trend is also true for irregular-wave cases, as illustrated in Fig. 8. In the irregular-wave case, the formulas for equivalent linearization are given by (8) and (9), and the values obtained for regular waves cannot directly be applied. In Fig. 8, in contrast to the case of linear pneumatic and viscous coefficients (Fig. 5), the chamber free-surface RAOs change even for slight variation of incident wave heights. In case of Hs = 1 m, the actual quadratic case gives slightly higher values than the linear equivalent ones but for Hs = 1.5 m, the trend is reversed.
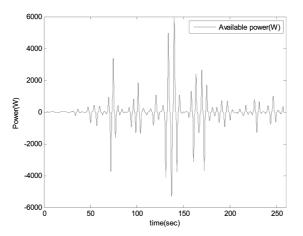
Fig. 10 Time histories of available power with quadratic coefficients ($D_{dm} = 0.004$, $v_{quad} = 500$) PM spectrum ($T_p = 5.5$, Hs = 1 m)
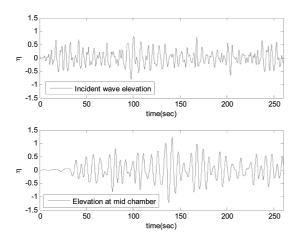

Fig. 11 Time histories of incident irregular waves (upper) and free surface at chamber midpoint (lower) with quadratic coefficients ($D_{dm} = 0.004$, $v_{quad} = 500$), PM spectrum ($T_p = 6.5$, Hs = 1 m)
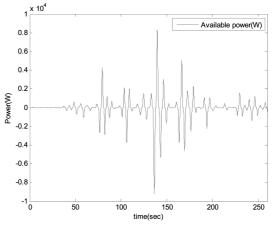

Fig. 12 Time histories of available power with quadratic coefficients ($D_{dm} = 0.004$, $v_{quad} = 500$), PM spectrum ($T_p = 6.5$, Hs = 1 m)

Finally, Figs. 9-12 show the time histories of the incident irregular wave and free surface at chamber midpoint, and the corresponding hydro-dynamically available power (work done by the chamber pressure force) of Fig. 8 case (Hs = 1 m) for two different incident wave spectra. The up-and-down movement of chamber water column for $T_p = 6.5$ s is greater than that of $T_p = 5.5$ s since the former is closer to the chamber resonance period. The large fluctuation of the available power in irregular waves imposes a serious challenge for future advancement of the present concept.

4. Conclusions

A time-domain simulation of a land-based Oscillating Water Column (OWC) with various

irregular waves is performed by using a two-dimensional fully nonlinear numerical wave tank (NWT). The NWT is based on potential theory, the mixed Eulerian-Lagrangian (MEL) time-marching approach, and the boundary element method. The nonlinear free-surface condition inside the OWC chamber was specially devised to describe both the pneumatic effect of the time-varying pressure and the viscous energy loss due to water column motions. The frontal damping zone is also specially devised to prevent re-reflected irregular waves from the wave maker to realize the true open-boundary condition.

The developed fully nonlinear NWT is applied to OWCs for irregular waves with nonlinear pneumatic and viscous parameters. It is also applied for both regular and irregular waves with equivalent linear coefficients to check the validity of such a simplified procedure. The trend of OWC performance for irregular waves generally follows that of regular waves but they are not necessarily identical because of various nonlinear effects. It is also seen that the results with equivalent linear coefficients show reasonable comparisons both in regular and irregular waves against nonlinear cases if incident waves are not highly nonlinear.

Acknowledgements

References

Gato, L.M.C. and Falcão, A.F.deO. (1988), "Aerodynamics of the wells turbine", *Int. J. Mech. Sci.*, **30**(6), 383-395.

Heath, T., Whittaker, T.J.T. and Boake, C.B. (2000), "The design, construction and operation of the LIMPET wave energy converter (Islay, Scotland)", *Proceedings of the 4th European Wave Energy Conf.*, Aalborg, Denmark.

Josset, C. and Clement, A.H. (2007), "A time-domain numerical simulator for oscillating water column wave power plants", *Renew. Energ.*, **32**(8), 1379-1402.

Kim, M.H. and Koo, W.C. (2005), *2D fully nonlinear numerical wave tanks*, *Numerical Models in Fluid Structure Interaction*, Ch.2, WIT Press.

Koo, W.C. and Kim, M.H. (2004), "Freely floating-body simulation by a 2D fully nonlinear numerical wave tank", *Ocean Eng.*, **31**(16), 2011-2046.

Koo, W.C. and Kim, M.H. (2010), "Nonlinear time-domain simulation of a land-based oscillating water column", *J. Waterw. Port. C. - ASCE*, **136**(5), 276-285.

Koo, W.C. and Kim, M.H. (2011), "A time-domain simulation of an oscillating water column with irregular waves", *Proceedings of the 2011 World Congress on Advances in Structural Engrg. and Mech.(ASEM)*, Seoul, Korea.

Koo, W.C., Kim, M.H., Lee, D.H. and Hong, S.A. (2006), "Nonlinear time-domain simulation of pneumatic floating breakwater", *Int. J. Offshore Polar.*, **16**(1), 25-32.

Liu, Z., Hyun, B.S. and Hong, K.Y. (2008), "Application of numerical wave tank to OWC air chamber for wave energy conversion", *Proceedings of the 18th Int. Offshore and Polar Engrg. Conf.*, ISOPE, Vancouver, BC, Canada.

Masuda, Y. and Miyazaki,T. (1979), "Wave power electric generation study in Japan", *Proceedings of the Wave and Tidal Energy Symposium*, British Hydromechanics Research Associates, Paper C.

Suzuki, M. and Arakawa, C. (2000), "Guide vanes effects of Wells turbine for wave power generator", *Int. J. Offshore Polar.*, **10**(2), 153-159.

Tanizawa, K. and Naito, S. (1997), "A study on parametric roll motions by fully nonlinear numerical wave tank", *Proceedings of the 7th Int. Offshore and Polar Engrg. Conf.*, ISOPE, Honolulu, USA.